JOURNAL OF SOLID STATE CHEMISTRY 109, 338–344 (1994)

High-Temperature Electrical Characterization of Ga-Based Layered Cuprates

G. W. Tomlins, N.-L. Jeon, and T. O. Mason

Department of Materials Science and Engineering, Science and Technology Center for Superconductivity, Northwestern University, Evanston, Illinois 60208

and

D. A. Groenke, J. T. Vaughey, and K. R. Poeppelmeier

Department of Chemistry, Science and Technology Center for Superconductivity, Northwestern University, Evanston, Illinois 60208

Received March 26, 1993; in revised form August 2, 1993; accepted August 4, 1993

High-temperature electrical conductivity and Seebeck coefficient measurements were performed on single-CuO_2-layer $La_{1-x}Sr_{1+x}CuGaO_5$ (x = 0.1 and 0.13) and double-CuO_2-layer $Y_{1-x}Ca_xSr_2Cu_2GaO_7$ (x = 0, 0.1, 0.2, 0.4). The solubility range in $Y_{1-x}Ca_xSr_2Cu_2GaO_7$ is most likely $0 \le x \le 0.2$, whereas, only the x = 0.1 composition is stable in $La_{1-x}Sr_{1+x}CuGaO_5$. Carrier concentration is essentially independent of temperature and oxygen partial pressure in both systems. The defect structure is dominated by $p = [AE'_{RE}]$, where AE = alkaline earth and RE = La or Y. The conductivity, and therefore the mobility, is activated for x = 0 and x = 0.1 in $Y_{1-x}Ca_xSr_2Cu_2GaO_7$. Solid solubility limits and charge localization play major roles in the establishment of superconductivity in these phases. © 1994 Academic Press, Inc.

INTRODUCTION

It is widely recognized that high-T_c copper oxide superconductors consist of CuO_2 layers sandwiched between metal oxide layers which serve both as insulating separators and as charge reservoirs whose variable composition (e.g., by oxygenation and/or aliovalent doping) governs the carrier content on the CuO_2 planes. Examples include rock salt AE–O layers (AE = alkaline earth) in La_2CuO_4-based materials, Cu–O chains in $YBa_2Cu_3O_{7-x}$ and $YBa_2Cu_4O_8$, and Bi–O or Tl–O layers in the Bi- or Tl-based cuprates. This work focused on compounds with Ga–O_4 layers, i.e., the recently discovered single- and double-CuO_2-layer Ga-based cuprates (1–4).

Polycrystalline single-layer $LaSrCuGaO_5$ was initially prepared in our laboratory by solid state reaction of oxides/carbonates at 980°C (1). Subsequently, single crystals were grown from copper oxide-rich flux (2). Rietveld analysis of neutron powder and X-ray single crystal diffraction patterns proved that this material crystallizes in the orthorhombic, noncentrosymmetric space group *Ima*2 and is isostructural with brownmillerite, Ca_2FeAlO_5. The solubility range is reportedly quite narrow, $0.1 \le x \le 0.13$ in $La_{1-x}Sr_{1+x}CuGaO_5$, and the material is virtually oxygen stoichiometric, i.e., oxygen content is 5.01 ± 0.02 by Rietveld analysis of diffraction data and TGA. Although possessing the requisite CuO_2 planes and a large hole content, this material is not superconducting under any synthesis conditions, including high oxygen pressure treatment and is paramagnetic down to 4 K.

The double-CuO_2-layer, $RESr_2Cu_2GaO_7$, materials were independently developed in our laboratory (3), by Roth *et al.* (4), and by Cava *et al.* (5). Synthesis of single-phase polycrystalline materials for all of the rare earths from erbium to lanthanum plus yttrium was accomplished by lengthy firing at 960–980°C in air. The crystal structure, also space group *Ima*2, consists of double CuO_2 planes and is related to that of $YBa_2Cu_3O_{7-y}$, but with the Cu–O chains replaced by Ga–O_4 tetrahedra. Hole doping has been most successful in the $Y_{1-x}Ca_xSr_2Cu_2GaO_7$ system. The solubility limit is reported to be x = 0.25 (3) or between x = 0.15 and x = 0.2 (4) $YSr_2Cu_2GaO_7$ is paramagnetic down to 4 K, as are the solid solution compositions prepared under normal conditions. When hot isostatic pressed to 200–300 atm of oxygen in the range 910–925°C, however, dense pellets exhibited superconductivity with $T_c \sim$ 20–25 K and powder-annealed samples were obtained with T_c as high as 73 K (3). Best results were obtained with compositions beyond the solubility limit, i.e., $0.2 < x \le 0.4$. TGA and Rietveld analysis of diffraction data indicate that these materials are virtually oxygen stoichiometric, i.e., oxygen content ~7.0.

These studies raise some interesting questions concerning the Ga-based cuprates. Are the differences in behavior from the other layered cuprate superconductors due to

0022-4596/94 $6.00

the $Ga-O_4$ tetrahedral layers in these structures? Since they are oxygen stoichiometric, why does hole doping not produce superconductivity under normal processing conditions? Why does high oxygen pressure treatment result in superconductivity in the double-layer compound but not the single layer compound? What are the underlying point defect structures of these materials? What role does the solubility limit play in determining transport properties, including superconductivity?

This study was undertaken to address these questions by means of high-temperature electrical property measurement. It is well known that equilibrium conductivity and thermoelectric coefficient measurements can reveal much concerning the point defect structure and transport properties of transition metal oxides (6). Furthermore, these properties are often sensitive to solubility limits. Since we already possess a large high-temperature electrical property database for layered cuprates (7), it was easy to make informative comparisons with related copper oxides.

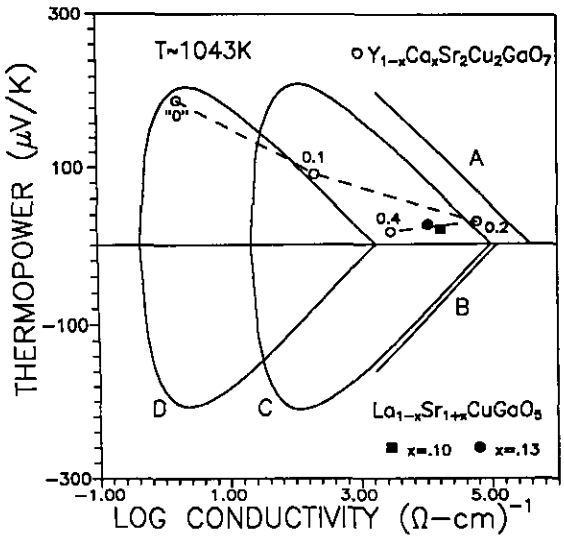

FIG. 1. Experimental thermopower-vs-conductivity plot at 1 atm oxygen and 1043 K. Schematic representation of Jonker data for $La_{2-x}Ba_xCuO_4$ (line A), $Nd_{2-x}Ce_xCuO_4$ (line B), $YBa_2Cu_3O_{7-x}$ (curve C), and $Bi_{2.1}Sr_{1.9}Ca_xY_{1-x}Cu_2O_8$ (curve D) from Refs. (6) and (8).

EXPERIMENTAL

Single CuO_2-layer specimens at $x = 0.1$ and $x = 0.13$ in $La_{1-x}Sr_{1+x}CuGaO_5$ were prepared by solid state reaction of La_2O_3 (Aldrich, 99.999%), $SrCO_3$ (Johnson Matthey, 99.999%), CuO (Aldrich, 99.999%), and Ga_2O_3 (Johnson Matthey, 99.999%) at 980°C for 1–2 weeks in air, with numerous intermediate grindings. The resulting air-cooled powders were single phase by X-ray diffraction. Powders were pressed into pellets and sintered at 990°C for 3–4 days to approximately 85–90% theoretical density. Rectangular conductivity specimens 3 × 3 × 15 mm were cut from the sintered pellets with a diamond saw.

The double-CuO_2-layer specimens at $x = 0$, 0.1, 0.2, and 0.4 in $Y_{1-x}Ca_xSr_2Cu_2GaO_7$ were prepared by solid state reaction of Y_2O_3 (Aldrich, 99.99%), $CaCO_3$ (Aldrich, 99.99%), $SrCO_3$ (Aldrich, 99.99%), Ga_2O_3 (Aldrich, 99.99%), and CuO (Aldrich, 99.999%) at 980°C for 3 weeks in air with frequent intermediate grindings. Except for the $x = 0.4$ composition, which had a significant amount of impurity phase, the other compositions were phase pure according to X-ray diffraction. As above, powders were pressed into pellets, sintered, and sectioned into 2 × 2 × 7-mm conductivity bars.

Simultaneous four-point electrical conductivity and thermoelectric coefficient measurements were made using the apparatus described previously (8). Current contacts were made by precious metal foils pressed against the ends of the specimen. Voltage contacts consisted of precious metal wire loops around the specimen, tied in place at notches along its length. One S-type thermocouple bead was in contact with each of the four leads. In this way six thermocouple combinations could be used to register steady-state emfs and the corresponding temperature differences for thermopower measurements. The specimen was placed just off the hot zone in the experimental furnace so as to yield a 10–20°C gradient along the length of the sample. Thermoelectric coefficients were corrected for the thermopower of platinum. A current reversal procedure was employed for conductivity measurements to subtract out thermal emf contributions. Platinum foils and wires were employed for the single-layer compound studies. These were replaced with gold for the double-layer compound studies to obviate the obvious reaction problems associated with platinum.

Although the four-point conductivity method eliminates contact resistance problems, grain boundaries often dominate the bulk conductivity of polycrystalline transition metal oxides. As a check for this, impedance spectra were measured over the frequency range 13 MHz to 5 Hz using a Hewlett–Packard 4192A frequency analyzer. No evidence of grain boundary effects was observed in the spectra.

The changes in electrical properties with temperature and oxygen pressure were small (see below). Nevertheless, measurements were taken only after steady state, indicating point defect equilibrium, had been achieved. This typically required 4–6 hr per datum.

RESULTS AND ANALYSIS

A. Jonker Analysis and Solubility Limits

We have previously shown that "Jonker pear" plots are useful for analyzing the high-temperature transport properties of cuprate superconductors (7). Figure 1 shows

a superposition of data for the single- and double-layer Ga-based cuprates and curves representing $La_{2-x}Ba_xCuO_4$ (A), $Nd_{2-x}Ce_xCuO_4$ (B), $YBa_2Cu_3O_{7-x}$ (C), and $Bi_{2.1}Sr_{1.9}Ca_xY_{1-x}Cu_2O_8$ (D). For semiconductors, thermopower is proportional to the logarithm of hole content by the constant $-k/e$ (-86.15 μV/K), where k is Boltzmann's constant and e is the unit of electron charge. Since conductivity should be proportional to the hole content (assuming constant mobility), a plot of thermopower vs log conductivity should yield a line with $-k/e$ slope, e.g., line A in the diagram. Similarly, electron doping should produce a line of $+k/e$ slope, e.g., line B in the diagram. In some systems a semiconducting p-to-n transition can be obtained at low doping levels, resulting in a complete "pear" as in curve C. This is the situation in $YBa_2Cu_3O_{7-x}$, where thermopower becomes progressively positive as oxygen content is reduced toward O_6 until the thermopower dramatically changes sign from positive to negative (7). Surprisingly, the curve is symmetric about the conductivity axis, indicating that the DOS (density of states)-mobility product is virtually identical for holes and electrons. In fact, the "point" of the "pear" indicates precisely this product, i.e., in order of decreasing DOS-μ product, $La_{2-x}Ba_2CuO_4$ (A) > $Nd_{2-x}Ce_xCuO_4$ (B) > $YBa_2Cu_3O_{7-x}$ (C) > $Bi_{2.1}Sr_{1.9}Ca_xY_{1-x}Cu_2O_8$ (D).

All of the systems exhibit deviations from linear behavior at high enough carrier contents. The $Bi_{2.1}Sr_{1.9}Ca_xY_{1-x}Cu_2O_8$ system is unique in this regard. Low Ca compositions fall neatly on curve D until approximately $x = 0.5$. Thereafter the data shift to progressively higher conductivities with Ca doping, reaching the point of curve C at the $x = 1$ composition (9). The double-layer Ga-based system behaves quite similarly to $Bi_{2.1}Sr_{1.9}Ca_xY_{1-x}Cu_2O_8$. This suggests that the DOS-μ product is small in the semiconducting state, but increases with doping. Owing to limited solid solubility, there are not enough data for the single-layer system to permit any conclusion about the DOS-μ product. Nevertheless, both single-layer compositions ($x = 0.1$, $x = 0.13$) appropriately fall between the $x = 0.1$ and $x = 0.2$ double-layer composition results.

The most significant aspect of Fig. 1 is the doubling back of the data for the highest doping level. We have previously demonstrated that high-temperature electrical properties can readily detect phase boundaries, i.e., the onset of phase decomposition (10). We attribute the reduction in conductivity from $x = 0.2$ to $x = 0.4$ in the double-layer system to the presence of second phases as detected by X-ray diffraction (3, 4). Similarly, the reduction in conductivity from $x = 0.1$ to $x = 0.13$ in the single-layer system suggests that the $x = 0.13$ composition is not phase pure, although it appears to be so by X-ray diffraction. Therefore, the solubility range is extremely narrow in $La_{1-x}Sr_{1+x}CuGaO_5$ and is restricted to approximately the $x = 0.1$ composition. On the other hand, Fig. 1 tends to confirm that the solubility range in the $Y_{1-x}Ca_xSr_2Cu_2GaO_7$ system is at least $0 \leq x \leq 0.2$.

B. Activation Energy Analysis

We restrict our attention in what follows to single-phase specimens only—$Y_{1-x}Ca_xSr_2Cu_2GaO_7$ ($x = 0$, 0.1, 0.2) and $La_{.9}Sr_{1.1}CuGaO_5$. Thermopower and electrical conductivity at 1 atm oxygen are plotted in Arrhenius fashion for the double-layer system in Figs. 2a and b, respectively. The data for the single-layer composition are plotted in Fig. 3.

In each case thermopower is approximately temperature independent. The most surprising feature is the evidence of an activated mobility for the $x = 0$ and $x = .1$ double-layer compositions. This is captured in Fig. 4, which plots the activation energies taken from Fig. 2b. Also plotted are activation energies from a standard small polaron plot of log σT vs T^{-1}. The behavior is not unlike what we previously reported in the $Nd_{2-x}Ce_xCuO_4$ system (11), although activation energy decreases much more gradually with increased doping in the Ga-based materials.

The behavior in Fig. 4 suggests a transition from small polaron behavior to metallic behavior as doping increases. This transition is gradual, however. In Fig. 5 we compare the thermopower at 1000 K and 1 atm oxygen for $Y_{1-x}Ca_xSr_2Cu_2GaO_7$ with a number of small polaron models (12). The "high" curves represent the localization of holes,

$$Q = +k/e \ln[2(\gamma - x)/x], \quad [1]$$

whereas the "low" curves represent the localization of electrons,

$$Q = -k/e \ln[2x/(\gamma - x)], \quad [2]$$

where x is Ca composition, $\gamma = 1$ or 2, and k/e are defined as above. In these equations we have neglected any entropy of transport contributions. None of the models correctly predicts the magnitude of the experimental behavior; however, the shape of the data closely follows that of the "electron" small polaron equation with $\gamma = 1$. The difference could be attributed to a nonzero entropy of transport term. The most important aspect of Fig. 5 is the evidence it provides for a gradual transition from localized to itinerant electronic behavior as doping increases.

C. Defect Structure Analysis

Every one of the phase-pure single- and double-layer compositions exhibited electrical properties which were virtually independent of oxygen pressure. For example, the conductivity of undoped $YSr_2Cu_2GaO_7$ is plotted in

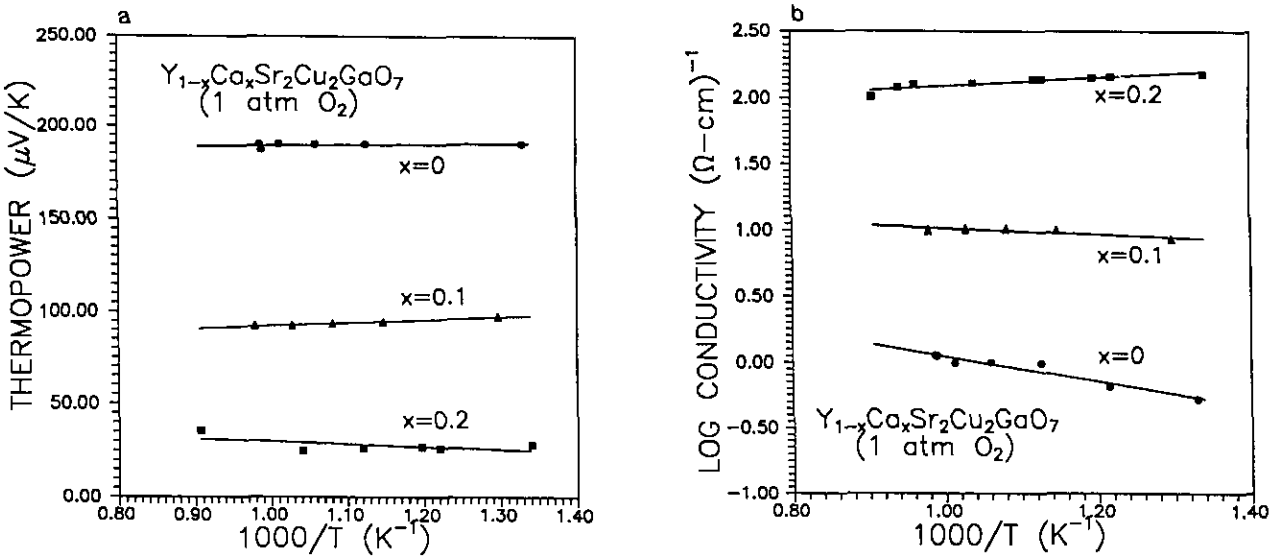

FIG. 2. Arrhenius plot of (a) thermopower and (b) electrical conductivity for $Y_{1-x}Ca_xSr_2Cu_2GaO_7$ compositions at 1 atm oxygen.

Fig. 6. The oxygen partial pressure dependence is $\sim+1/50$, indicative of hole-type character, but nearly independent of oxygen pressure. Other compositions in $Y_{1-x}Ca_xSr_2Cu_2GaO_7$ (x = 0.1, 0.2) and $La_{.9}Sr_{1.1}CuGaO_5$ behaved similarly.

In order to understand this behavior in terms of defect structure, it is necessary to review what is known about the defect structure of a related cuprate system, $La_{2-x}Ba_xCuO_{4\pm\delta}$ (6). Specific point defect regimes are traversed as doping increases. Undoped and slightly doped compositions exhibit electrical properties which are independent of doping composition but which are proportional to the $\frac{1}{6}$ power of oxygen pressure. This has been attributed to the presence of oxygen interstitials according to

$$\tfrac{1}{2}O_2(g) \rightleftharpoons O_i'' + 2h\cdot; \quad K_{ox}p_{O_2}^{1/2} = [O_i'']p^2. \qquad [3]$$

With increased doping this regime gives way to an aliovalent doping regime, where

$$p = [Ba_{La}'] \qquad [4]$$

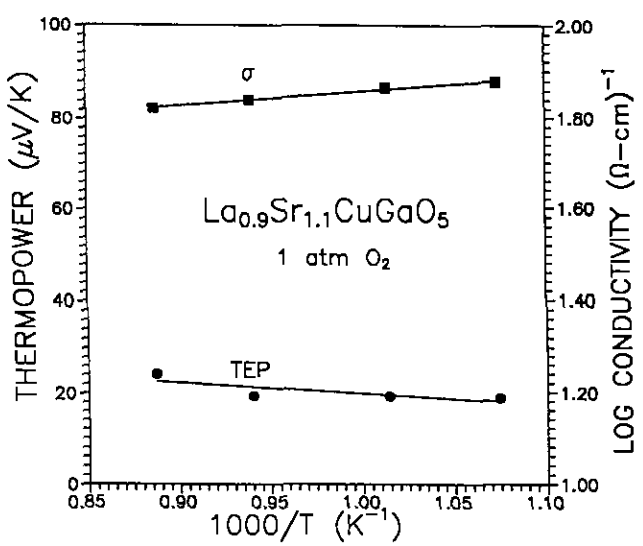

FIG. 3. Arrhenius plot of thermopower and electrical conductivity for $La_{0.9}Sr_{1.1}CuGaO_5$ at 1 atm oxygen.

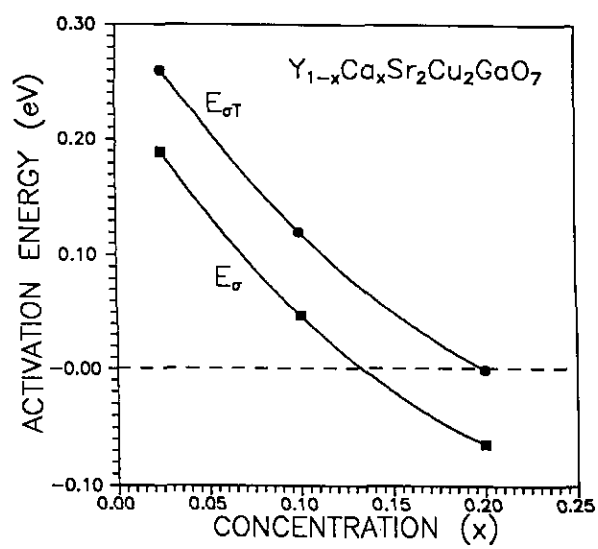

FIG. 4. Unmodified (σ) and small polaron (σT) activation energies for $Y_{1-x}Ca_xSr_2Cu_2GaO_7$ compositions at 1 atm oxygen.

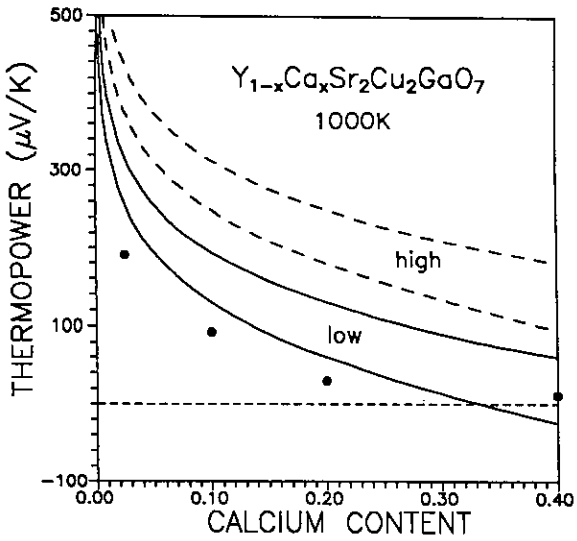

FIG. 5. Thermopower at 1 atm oxygen and 1000 K vs calcium content in the $Y_{1-x}Ca_xSr_2Cu_2GaO_7$ system. See text for explanation of "high" and "low" curves.

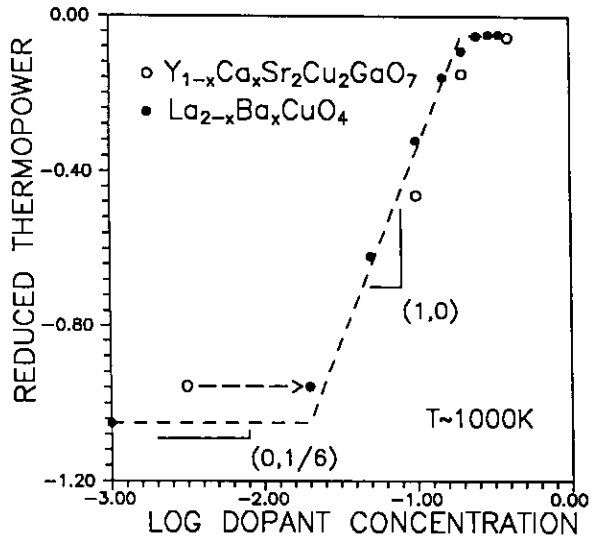

FIG. 7. Reduced thermopower (hole content) vs dopant concentration in $Y_{1-x}Ca_xSr_2Cu_2GaO_7$ vs $La_{2-x}Ba_xCuO_4$ (data from Ref. 6). See text for explanation of slopes.

and the oxygen pressure dependence is negligible. This behavior is captured in Fig. 7, where reduced thermopower ($-Qe/2.303k$), which should be proportional to the logarithm of the hole concentration, is plotted vs the logarithm of dopant concentration. The oxygen interstitial regime is labeled with a slope of (0, $\frac{1}{6}$), where the first number indicates the dopant dependence and the second indicates the oxygen pressure dependence. The second, impurity-controlled, regime is labeled with the slope (1, 0), where 1 reflects the electroneutrality condition of Eq. [4] and the 0 shows that there is little or no oxygen pressure dependence. The $La_{2-x}Ba_xCuO_{4\pm\delta}$ behavior exemplifies both point defect regimes. (A third point defect regime occurs at larger doping levels (6), beyond the solubility limits of the Ga-based phases, and is not considered here.)

With the exception of the $x = 0.4$ sample, which is not single phase, the Ga-based cuprates appear to exhibit impurity-controlled, second-regime behavior, including the "undoped" specimen. There is little or no oxygen partial pressure dependence, and hole content increases linearly with dopant concentration. Agreement with the $La_{2-x}Ba_xCuO_{4\pm\delta}$ data is noteworthy.

The behavior of the undoped specimen cannot be explained on the basis of Ca doping. This sample is arbitrarily given a log [Ca] value of −2.5 in Fig. 7. The dashed arrow indicates where the true hole content must lie, based upon our knowledge that this sample exhibits impurity-controlled behavior. The hole content corresponding to the thermopower would be between 0.02 and 0.025. (Note that an "effective" calcium content of 0.025 was employed in Fig. 5.) Possible explanations for the origin of holes in undoped $YSr_2Cu_2GaO_7$ are given below.

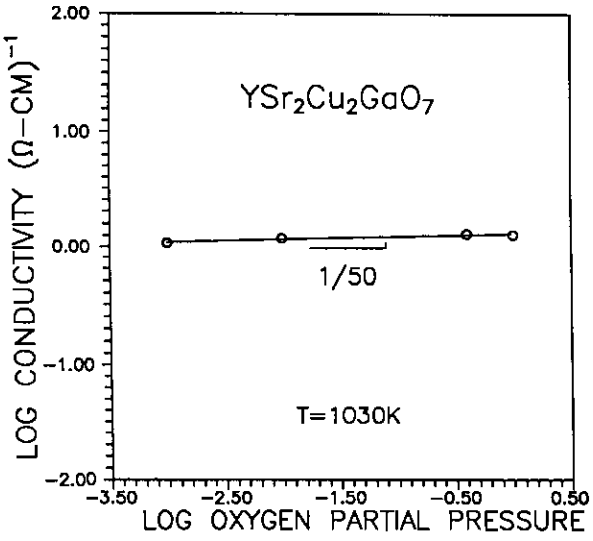

FIG. 6. Oxygen partial pressure dependence of electrical conductivity for $YSr_2Cu_2GaO_7$ at 1 atm oxygen and 1030 K.

DISCUSSION

The single- and double-CuO_2-layer Ga-based materials are not significantly different in high-temperature electrical properties from the other layered cuprates. In fact, the "Jonker plot" of $Y_{1-x}Ca_xSr_2Cu_2GaO_7$ nearly replicates that of $Bi_{2.1}Sr_{1.9}Ca_xY_{1-x}Cu_2O_8$. It is therefore not

surprising to find that $Y_{1-x}Ca_xSr_2Cu_2GaO_7$ can be made to superconduct by high oxygen pressure treatments. Where the Ga-based phases differ from the other cuprates is in their restricted solubility ranges and in their tendency for charge localization, especially in $Y_{1-x}Ca_xSr_2Cu_2GaO_7$.

The stability range of $Y_{1-x}Ca_xSr_2Cu_2GaO_7$ is most likely $0 \leq x \leq 0.2$ (3, 4), whereas $La_{1-x}Sr_{1+x}CuGaO_5$ appears to be stable only at or very near $x = 0.1$. The latter doping level is significantly below the optimal hole content for superconductivity in other layered cuprates, e.g., approximately 0.16 in $La_{2-x}AE_xCuO_4$. This may explain why $La_{1-x}Sr_{1+x}CuGaO_5$ compositions at or beyond the solubility limit cannot be made to superconduct by high oxygen pressure treatment. On the other hand, such treatment of $x > 0.2$ in $Y_{1-x}Ca_xSr_2Cu_2GaO_7$ results in superconducting phases. High-pressure annealed samples show a decreased amount of impurity phase(s) and a noticeable contraction of the in-plane lattice parameters, indicating an increased hole doping of the CuO_2 planes. This suggests that the solubility limit is a favorable function of oxygen pressure in $Y_{1-x}Ca_xSr_2Cu_2GaO_7$, whereas it is not in $La_{1-x}Sr_{1+x}CuGaO_5$. High-pressure phase equilibrium studies would be required to establish whether or not this is the case.

The charge carriers in $Y_{1-x}Ca_xSr_2Cu_2GaO_7$ exhibit activated mobilities at high temperatures for at least $0 \leq x \leq 0.1$. This indicates a strong tendency for charge localization. The most noteworthy feature is the persistence of such localization to large doping levels in contrast to the other layered cuprates we have studied. Localization may be responsible for the fact that as-synthesized specimens are not superconducting. This contention is supported by recent transmission electron energy loss spectrometry on $Y_{1-x}Ca_xSr_2Cu_2GaO_7$ samples (13). In as-synthesized specimens, a broad pre-edge feature below the O–K absorption edge emerges with Ca doping at about 528.8 eV. Upon high-pressure O_2 annealing, a second smaller pre-edge feature (at 527.1 eV) emerges and grows at the expense of the 528.8-eV feature. Both features were interpreted as being associated with holes, the former being bound in some way and the latter being responsible for superconductivity. There is an apparent transfer of charge from bound to free states as a result of high oxygen pressure treatment, as evidenced by the EELS data and the observed contraction of in-plane lattice parameters (3).

The defect structure of *doped* $Y_{1-x}Ca_xSr_2Cu_2GaO_7$ is not as complicated as some of the other layered cuprates. Oxygen defects, e.g., vacancies and interstitials, do not seem to play as major a role; these materials are largely oxygen stoichiometric. Aliovalent doping plays the dominant role, with Ca'_Y being compensated by electron holes. The only unusual feature in this system is the tendency for charge carrier localization as discussed above.

The defect behavior of undoped $YSr_2Cu_2GaO_7$ is somewhat anomalous. It is difficult to account for the large hole content and associated electrical properties (high conductivity and small thermopower) in what should be an insulating composition. Simple disorder of cations between Y and Sr sites, e.g., $[Y^{\cdot}_{Sr}] = [Sr'_Y]$, as observed for $RESr_2Cu_2GaO_7$ compuonds with larger *RE* ions (4), would have no impact on the electroneutrality condition. A more likely explanation involves cation vacancies on *RE* or *AE* sites. For example, a Sr vacancy population of 0.01 would require a hole content of 0.02 if $p = 2[V''_{Sr}]$. Studies of the compositions $YSr_{2-x}Cu_2GaO_7$ as a function of x are currently underway to test this hypothesis.

CONCLUSIONS

High-temperature electrical property (conductivity, thermopower) studies have shown that solid solubility extends to at least $x = 0.2$ in $Y_{1-x}Ca_xSr_2Cu_2GaO_7$. The undoped ($x = 0$) and $x = 0.1$ compositions exhibit activated conductivity while thermopower remains essentially independent of temperature. This indicates an activated mobility associated with charge localization. The defect structure in $Y_{1-x}Ca_xSr_2Cu_2GaO_7$ is dominated by the aliovalent doping of yttrium sites, i.e., $p = [Ca'_Y]$. Undoped $YSr_2Cu_2GaO_7$ exhibits extrinsic defect behavior, presumably a result of unintentional cation vacancies. Similar high-temperature electrical studies of $La_xSr_{1+x}CuGaO_5$ suggest that the phase is only stable in the vicinity of $x = 0.1$. As in the $Y_{1-x}Ca_xSr_2Cu_2GaO_7$ system, electrical properties are independent of oxygen partial pressure, suggesting that aliovalent doping, i.e., $p = [La'_{Sr}]$, governs the defect structure.

In conclusion it appears that charge localization and the limited solubility ranges are important factors in explaining why it is difficult to achieve superconductivity in these Ga-based phases.

ACKNOWLEDGMENTS

This work was supported by the Science and Technology Center for Superconducivity under NSF Grant DMR-91-20000 and is based, in part, on the B.S. senior project of N.-L. Jeon and on the M.S. dissertation of G. W. Tomlins. Portions of the research were carried out in facilities of the Materials Research Center under Grant no. NSF-MRL-9120521.

REFERENCES

1. J. T. Vaughey, R. Shumaker, S. N. Song, J. B. Ketterson, and K. R. Poeppelmeier, *Mol. Cryst. Liq. Cryst.* **184,** 335 (1990).
2. J. T. Vaughey, J. B. Wiley, and K. R. Poeppelmeier, *Z. Anorg. Allg. Chem.* **598/599,** 327 (1991).
3. J. T. Vaughey, J. P. Thiel, E. F. Hasty, D. A. Groenke, C. L. Stern, K. R. Poeppelmeier, B. Dabrowski, D. G. Hinks, and A. W. Mitchell, *Chem. Mater.* **3,** 935 (1991); B. Dabrowski, P. Padaelli, D. G. Hinks, A. W. Mitchell, J. T. Vaughey, D. A. Groenke, and K. R. Poeppelmeier, *Physica C* **193,** 63 (1992).

4. G. Roth, P. Adelmann, G. Heger, R. Knitter, and Th. Wolf, *J. Phys. I* **1,** 721 (1991).
5. R. J. Cava, R. B. Van Dover, B. Batlogg, J. J. Krajewski, L. F. Schneemeyer, T. Siegrist, B. Hessen, S. H. Chen, W. F. Peck, Jr., and L. W. Rupp, Jr., *Physica C* **185–198,** 180 (1991).
6. T. O. Mason, *in* "Electronic Ceramic Materials" (J. Nowotny, Ed.), p. 502. Trans Tech Publications, Zürich, 1992.
7. M.-Y. Su, C. E. Elsbernd, and T. O. Mason, *J. Am. Ceram. Soc.* **73**(2), 415 (1990).
8. A. Trestman-Matts, S. E. Dorris, and T. O. Mason, *J. Am. Ceram. Soc.* **66**(8), 589 (1983).
9. B.-S. Hong and T. O. Mason, *J. Am. Ceram. Soc.* **76**(3), 635 (1993).
10. B.-S. Hong and T. O. Mason, *J. Mater. Res.* **6**(10), 2054 (1991).
11. M.-Y. Su, C. E. Elsbernd, and T. O. Mason, *Physica C* **21,** 114 (1989).
12. J. Nell, B. J. Wood, S. E. Dorris, and T. O. Mason, *J. Solid State Chem.* **83,** 247 (1989).
13. V. P. Dravid and H. Zhang, *Physica C* **200,** 349 (1992).